Journal of Inflammation Research

Dovepress
open access to scientific and medical research

Open Access Full Text Article

ORIGINAL RESEARCH

Differential Diagnosis of Nonabsorbable Inflammatory and Malignant Subsolid Nodules with a Solid Component ≤5 mm

Xiao-Qun He[1,*], Xian Li[2,*], Yan Wu[3], Shun Wu[1], Tian-You Luo[1], Fa-Jin Lv[1], Qi Li[1]

[1]Department of Radiology, The First Affiliated Hospital of Chongqing Medical University, Chongqing, People's Republic of China; [2]Department of Pathology, Chongqing Medical University, Chongqing, People's Republic of China; [3]Nursing School, Chongqing Medical University, Chongqing, People's Republic of China

*These authors contributed equally to this work

Correspondence: Qi Li, Department of Radiology, The First Affiliated Hospital of Chongqing Medical University, No. 1 Youyi Road, Yu Zhong District, Chongqing, 400016, People's Republic of China, Tel +86 15823408652, Fax +86 23 68811487, Email liqi89011721@163.com

Purpose: To investigate the differential clinical and computed tomography (CT) characteristics of pulmonary nonabsorbable inflammatory and malignant subsolid nodules (SSNs) with a solid component ≤5 mm.

Patients and Methods: We retrospectively analyzed 576 consecutive patients who underwent surgical resection and had SSNs with a solid component ≤5 mm on CT images. These patients were divided into inflammatory and malignant groups according to pathology. Their clinical and imaging data were analyzed and compared. Multiple logistic regression analysis was used to identify independent prognostic factors differentiating inflammatory from malignant SSNs. Furthermore, 146 consecutive patients were included as internal validation cohort to test the prediction efficiency of this model.

Results: Significant differences in 11 clinical characteristics and CT features were found between both groups ($P < 0.05$). Presence of respiratory symptoms, distribution of middle/lower lobe, irregular shape, part-solid nodule (PSNs), CT value of ground-glass opacity (GGO) areas <−657 Hu, presence of abnormal intra-nodular vessel sign, and interlobular septal thickening were the most effective factors for diagnosing nonabsorbable inflammatory SSNs, with an AUC (95% CI), accuracy, sensitivity, and specificity of 0.843 (95% CI: 0.811–0.872), 89.76%, 72.86%, and 81.23%, respectively. The internal validation cohort obtained an AUC (95% CI), accuracy, sensitivity, and specificity of 0.830 (95% CI: 0.759–0.887), 83.56%, 73.91%, and 76.42%, respectively.

Conclusion: Nonabsorbable inflammatory and malignant SSNs with a solid component ≤5 mm exhibited different clinical and imaging characteristics.

Keywords: subsolid nodule, ground-glass opacity, computed tomography, pathology

Introduction

Clinicians around the world frequently encounter pulmonary subsolid nodules (SSNs) during lung cancer screening using computed tomography (CT), which also poses a diagnostic challenge to radiologists. SSN is a morphological description for various pulmonary nodules, including pure ground-glass nodules (pGGNs) and part-solid nodules (PSNs), the latter of which contain both ground-glass opacity (GGO) and solid opacity.[1–4]

Previous studies have indicated that SSNs, particularly PSNs, are considered to have a higher potential for malignancy than do solid pulmonary nodules of a similar size.[2,5] However, it is worth mentioning that SSN is a non-specific finding, and some inflammatory entities, such as focal inflammation, focal fibrosis, and organizing pneumonia, can also manifest as this pattern.[6] Generally, most inflammatory SSNs may disappear on follow-up CT examinations. Therefore, it is usually recommended that patients with nonabsorbable SSNs receive surgical treatment after a period of follow-up CT. This may cause unnecessary surgery of nonabsorbable inflammatory SSNs. Ye et al[7] retrospectively evaluated 736 patients with SSNs undergoing a surgical procedure; of these SSNs, 7.4% turned out to be benign.[8] Some

Received: 26 December 2021
Accepted: 1 March 2022
Published: 11 March 2022

investigators have indicated that surgical operation may damage pulmonary function, even in cases of wedge or segmental resection.[9,10] Hence, imaging differentiation of nonabsorbable inflammatory and malignant SSNs preoperatively is crucial in minimizing overtreatment and making optimal treatment decisions.

Currently, CT is the preferred imaging modality for the screening and diagnosis of SSNs. 2015 WHO classification defined SSNs with invasive component ≤5 mm as preinvasive lesions and minimally invasive adenocarcinoma (MIA).[11] Previous studies have found a significant correlation between the size of the solid component on thin-section CT and the invasive component on pathology for SSNs.[12,13] Some investigators in the field have proposed the development of clinical and CT guidelines for discriminating between inflammatory and malignant SSNs. However, to date, most studies have focused on the differential diagnosis between inflammatory and invasive SSNs, and few have sought to study the differential diagnosis between inflammatory and preinvasive or minimally invasive SSNs.

Therefore, this study aimed to compare the clinical and CT features that distinguish nonabsorbable inflammatory SSNs, which was defined as nodules persistent for more than three months on follow-up CT without any decrease in size here, from malignant SSNs with a solid component ≤5 mm.

Patients and Methods

Patient Selection

Our hospital's institutional review board approved this study, and the need for informed consent was waived due to its retrospective nature. Meanwhile, this study was conducted in accordance with the Declaration of Helsinki, and used anonymous data and had no potential risks to patients. For this retrospective study, 604 consecutive patients between August 2018 and November 2020 were initially included. These patients fulfilled the following inclusion criteria:1) patients undergoing chest CT scan; 2) patients with a nodule manifesting as SSN with the largest solid-component dimension ≤5 mm in the lung window setting (window width, 1600 Hounsfield units; window level, −600 Hounsfield units); 3) SSNs persistent for more than three months on follow-up CT without any decrease in size; 4) nodules were surgically resected and confirmed pathologically. Twenty-eight patients were excluded because the size of the solid component within the SSN was difficult to measure accurately via CT. In total, 576 patients were finally included. These patients were divided into inflammatory and malignant groups based on pathological results. We also recorded patients' clinical characteristics, including age, sex, smoking history, and respiratory symptoms. Furthermore, 146 consecutive patients from December 2020 to February 2021 who met the inclusion and exclusion criteria were included as the internal validation cohort.

CT Protocol

Non-contrast chest CT examinations were performed using a Discovery 750 HD CT (GE Healthcare, Milwaukee, WI, USA); Somatom Perspective (GE Healthcare, Erlangen, Germany); or Somatom Definition FLASH (Siemens Healthcare, Forchheim, Germany) CT scanner. Patients were all placed in a supine position and scanned in the craniocaudal direction. CT scanning was first conducted at the end of inspiration during a single breath-hold, from the thoracic inlet to immediately below the costophrenic angle, with the following parameters: tube voltage of 110–120 kVp, tube current of 50–250 mAs (automatic tube current modulation technology), rotation time of 0.5 s, pitch of 0.875–1.50, slice thickness of 5 mm, and interval of 5 mm on axial images. Subsequently, images were reconstructed with a slice thickness of 0.625–1.25 mm and a slice interval of 0.625–1.25 mm, standard filtered back projection algorithm involving a kernel of high spatial resolution and displayed with a standard lung window setting.

CT Image Interpretation

Two chest radiologists (with 20 and 13 years of experience in chest CT imaging, respectively) who were blinded to patient data interpreted the images together, and decisions on CT findings were reached through consensus. CT morphological features of each nodule were carefully analyzed as follows:

1. size (maximum diameter of nodules in the lung window setting)

2. distribution (upper or middle and lower lobes)
3. shape (regular [round or oval] or irregular [with an uneven contour that could not be classified as round or oval] [Figure 1A and B])
4. margin (well-defined [clear border definition] or ill-defined [partially or completely blurred border definition] [Figure 1A and B])
5. intra-nodular characteristics, including density (pGGN and PSN [Figure 1C and D]); CT value of GGO areas (measurement method: the largest slice of SSN for each patient was selected from axial CT images in the lung window. For pGGNs, a circular region of interest (ROI) was drawn to include more than two-thirds of the entire nodule, while for PSNs, a circular ROI as large as possible was placed on GGO regions of the nodule cautiously avoiding solid component, vessels, and bronchi. To reduce error, the same ROI was placed on three adjacent images using a copy-and-paste function, and the average values were calculated as CT value of GGO areas [Figure 1C and D]); target sign (characterized by a focal and round-like solid component in the center of GGO-predominant nodule, similar to a target [Figure 1E]); bubble lucency (round or oval air attenuation within lesions [Figure 1F]); air bronchogram (branched or tubular air structure within lesions [Figure 1G]); intra-nodular vessel sign (vessels passing through nodules [Figure 1H]); and abnormal intra-nodular vessel sign (vessels in the nodule manifesting as dilatation, distorting, or increased branches. Dilatation was defined as increased vascular diameter by comparing with that of other vessels of the same grade in the identical or other lung lobes [Figure 1I].

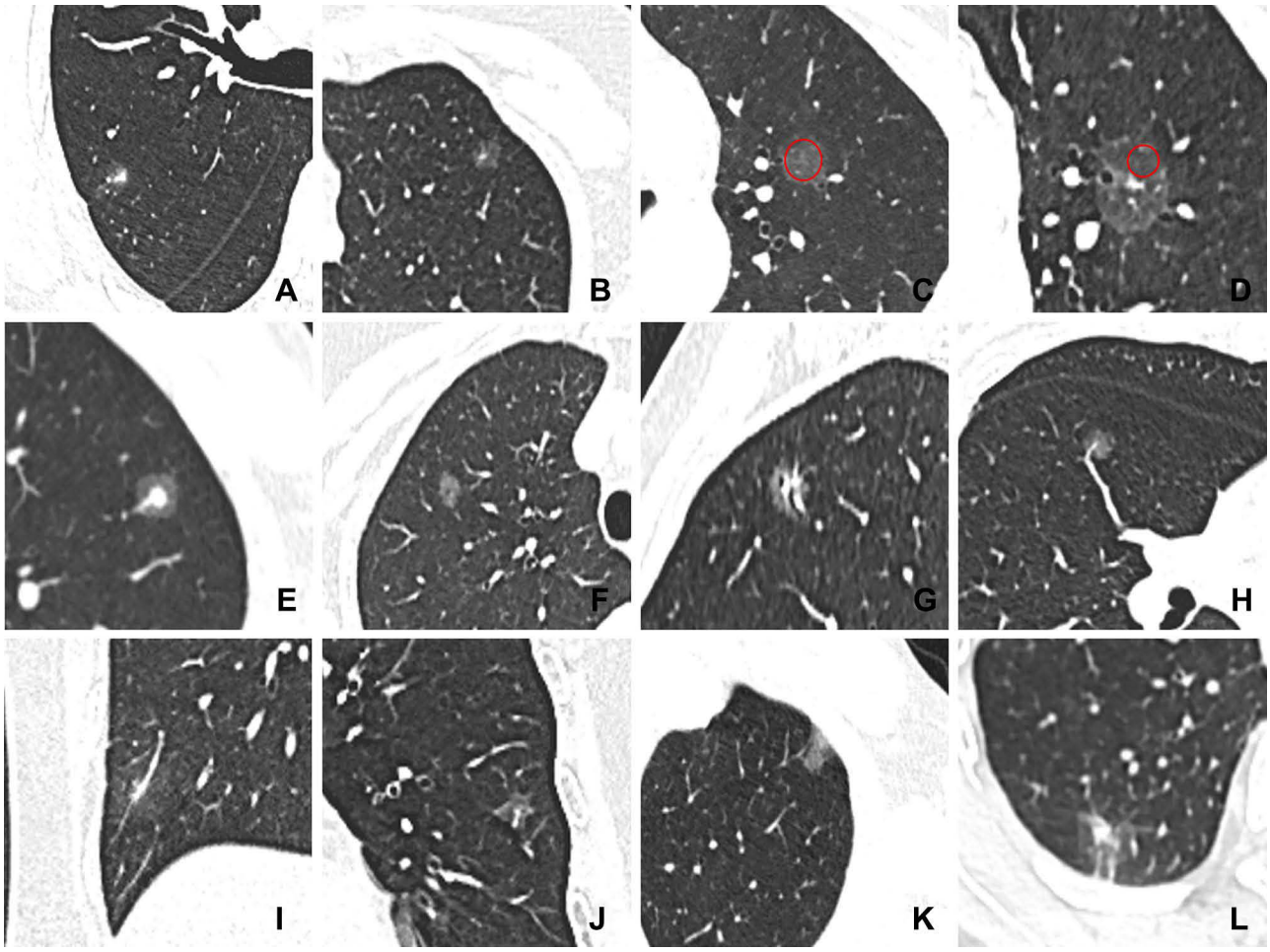

Figure 1 Representative images of CT features. (**A**) SSN with irregular shape and ill-defined margin; (**B**) SSN with regular shape and well-defined margin; (**C**) measurement of CT value of GGO areas for pGGN (red circle); (**D**) measurement of CT value of GGO areas for PSN (red circle); (**E**) SSN with target sign; (**F**) SSN with bubble lucency; (**G**) SSN with air bronchogram; (**H**) SSN with intra-nodular vessel sign; (**I**) SSN with abnormal intra-nodular vessel sign; (**J**) SSN with thickened interlobular septa; (**K**) SSN with pleural attachment; (**L**) SSN with pleural retraction.

Distorting was defined as curving of the vessels within the nodule. Increased branches were identified by comparing with those of adjacent vessels of the same grade).

6. Extra-nodular characteristics, including thickened interlobular septa [Figure 1J], pleural changes (pleural attachment [lesion attached to the pleura with the margin obscured by the pleura] [Figure 1K] and pleural retraction [linear structures connected between the tumor and pleura] [Figure 1L]).

For patients with sequential CT scans, image analyses were based on data from the final CT scan taken before treatment commenced.

Pathological Evaluation

All patients received sub-lobar resection or lobectomy. The specimens were fixed in 10% formalin, sliced at the maximum dimension, embedded in paraffin, sectioned with a microtome, and then stained with hematoxylin and eosin. A senior pathologist (X.L., with 13 years of experience in pathological diagnosis of the lung diseases) who was blinded to patient data evaluated all existing histopathological slides. Pathological analysis of nodules was identified according to the recently updated World Health Organization (WHO) classification (2015) and the eighth edition of the American Joint Committee on Cancer staging system for non-small cell lung cancer (2017).[12,14,15]

Statistics Analysis

Statistical analyses were performed using a statistical software package (SPSS, version 21.0 for Windows; IBM; NY, USA). Firstly, continuous variables were tested for normality using Kolmogorov–Smirnov analysis. Normally distributed quantitative data were expressed as mean ± standard deviation and analyzed using the Two-independent-samples Student's *t*-test, whereas non-normally distributed data were presented as median ± interquartile range and assessed using the Mann–Whitney *U*-test. Categorical variables were expressed as numbers and percentages and evaluated using the Chi-squared test. The Youden Index was calculated to establish the optimal threshold values of CT value of GGO areas. For comparison of clinical and CT features, a two-sided P value < 0.05 was considered to indicate a significant difference. Moreover, the diagnostic consistency was assessed using intraclass correlation coefficients (ICCs) for quantitative data and Kappa test for qualitative variables. ICCs > 0.75 and Kappa value > 0.80 show a good agreement between two observers.

Multivariable logistic regression analysis was then applied using clinical and CT features that differed significantly between both groups to select independent predictors in discriminating between nonabsorbable inflammatory and malignant SSNs. The final regression model was selected using the forward condition method, and the area under the receiver operating characteristic curve (AUC), accuracy, sensitivity, and specificity were used to evaluate diagnostic performance.

Results

Observer Reproducibility

The agreement among two observers was fairly good for all CT features. The ICCs values of diagnostic tests for tumour size and CT value of GGO areas were 0.975 and 0.985 (all $P < 0.001$), respectively. Additionally, Kappa values for distribution, shape, margin, density, target sign, bubble lucency, air bronchogram, intra-nodular vessel sign, abnormal intra-nodular vessel sign, thickened interlobular septa, and pleural changes between two observers were 1.00, 0.905, 0.868, 0.969, 0.942, 0.955, 0.912, 0.935, 0.885, 0.921 and 0.967 (all $P < 0.001$), respectively.

Study Population

A total of 576 nodules [median size of 10.30 (9.00, 13.00) mm and range of 8.00–30.00 mm] in 576 patients [median age of 54 (46, 62) years and range of 23–87 years] were identified in this study. Seventy patients (12.15%, 70/576) were confirmed as having nonabsorbable inflammatory nodules and 506 patients (87.85%, 506/576) were diagnosed as having malignant SSNs; the latter included 184 cases of AIS and 322 cases of MIA. Furthermore, 23 patients with

nonabsorbable inflammatory SSNs and 123 patients with malignant SSNs with a solid component ≤5 mm were included as internal validation cohort.

Clinical Characteristics

Table 1 shows the clinical characteristics of patients in both groups. Malignant SSNs were more frequently observed in women and non-smokers, whereas respiratory symptoms were more common in patients with inflammatory SSNs (all $P < 0.05$). However, no significant difference in age was observed between the two groups ($P > 0.05$).

CT Manifestations

Table 2 illustrates the CT features of the observed SSNs in both groups. The median size was 11.00 (9.00, 14.00) mm and 10.00 (9.00, 13.00) mm in inflammatory and malignant SSNs, respectively, and no significant difference was found between the two groups ($P > 0.05$). Distribution of upper lobe, regular shape, and well-defined margin were more frequently observed in the malignant group than those in the inflammatory group (all $P < 0.05$). With regard to intra-nodular and extra-nodular characteristics, malignant SSNs had a significantly higher frequency of pGGNs, whereas inflammatory SSNs had a significantly higher occurrence rate of target sign, abnormal intra-nodular vessel sign, and thickened interlobular septa (all $P < 0.05$). Furthermore, the CT value of GGO areas in malignant SSNs was higher than that in inflammatory ones ($P < 0.001$). The cutoff CT value of GGO areas for differentiating inflammatory from malignant SSNs was −657 Hu, with an AUC, sensitivity, and specificity of 0.711, 71.30%, and 62.90%, respectively. However, no significant differences were observed in bubble lucency, air bronchogram, intra-nodular vessel sign, and pleural changes between the two groups (all $P > 0.05$).

Multivariate Logistic Regression Analysis

Table 3 reveals the independent prognostic factors for diagnosing nonabsorbable inflammatory SSNs. For the model with clinical and CT features that differed significantly between both groups, presence of respiratory symptoms (odds ratio [OR] = 3.671, 95% confidence interval [CI]: 1.824–7.387), distribution of middle/lower lobe (OR = 4.134, 95% CI: 2.206–7.750), irregular shape (OR = 2.953, 95% CI: 1.389–6.277), PSNs (OR = 3.199, 95% CI: 1.708–5.991), CT value of GGO areas <−657 Hu (OR = 6.787, 95% CI: 3.566–12.919), presence of abnormal intra-nodular vessel sign (OR = 4.897, 95% CI: 2.350–10.201), and interlobular septal thickening (OR = 13.238, 95% CI: 2.581–67.906) were significantly associated

Table 1 Comparison of Clinical Characteristics Between Inflammatory and Malignant SSNs [n (%)]

Characteristics	Inflammatory SSNs (n = 70)	Malignant SSNs (n = 506)	*P* value
Age (years)	55 ± 13	54 ± 15	0.956[a]
Sex			
Female	30 (42.86)	326 (64.43)	< 0.001[b]
Male	40 (57.14)	180 (35.57)	
Smoking history			
Non-smoker	45 (64.29)	408 (80.63)	0.002[b]
Smoker	25 (35.71)	98 (19.37)	
Respiratory symptoms			
Presence of symptoms	23 (32.86)	70 (13.83)	< 0.001[b]
Cough	16	46	
Sputum	8	19	
Chest pain	10	30	
Wheezing	2	3	
Hemoptysis	0	5	
Fever	1	1	
Absence of symptoms	47 (67.14)	436 (86.17)	

Notes: [a]Mann–Whitney *U*-test; [b]Chi-squared test.
Abbreviation: SSNs, subsolid nodules.

Table 2 Comparison of CT Features Between Inflammatory and Malignant SSNs [n (%)]

Characteristics	Inflammatory SSNs (n = 70)	Malignant SSNs (n = 506)	*P* value
Distribution			
Upper lobe	38 (54.29)	376 (74.31)	<0.001[b]
Middle/lower lobe	32 (45.71)	130 (25.69)	
Lesion size (mm)	11.00 ± 9.00	10.00 ± 4.00	0.386[a]
Shape			
Regular	50 (71.43)	461 (91.11)	<0.001[b]
Irregular	20 (28.57)	45 (8.89)	
Margin			
Well-defined	27 (38.57)	281 (55.53)	0.008[b]
Ill-defined	43 (61.43)	225 (44.47)	
Intra-nodular characteristics			
Lesion density			
pGGNs	38 (54.29)	415 (82.02)	<0.001[b]
PSNs	32 (45.71)	91 (17.98)	
CT value of GGO areas (Hu)	-(678.00 ± 140.00)	-(598.00 ± 149.00)	<0.001[a]
Target sign	13 (18.57)	45 (8.89)	0.012[b]
Bubble lucency	11 (15.71)	81 (16.01)	0.950[b]
Air bronchogram	7 (10.00)	49 (9.68)	0.933[b]
Intra-nodular vessel sign	52 (74.29)	420 (83.00)	0.076[b]
Abnormal intra-nodular vessel sign	20 (28.57)	60 (11.86)	<0.001[b]
Extra-nodular characteristics			
Interlobular septal thickening	9 (12.86)	4 (0.79)	<0.001[b]
Pleural changes	25 (35.71)	143 (28.26)	0.198 [b]

Notes: [a]Mann–Whitney *U*-test; [b]Chi-squared test.
Abbreviations: SSNs, subsolid nodules; pGGNs, pure ground-glass opacity nodules; PSNs, part-solid nodules; CT, computed tomography; GGO, ground-glass opacity.

Table 3 Multivariable Logistic Regression Analysis of Independent Prognostic Factors for Predicting Nonabsorbable Inflammatory SSNs

Variables	B	S.E.	Wald	Odds Ratio (95% CI)	*P* value
Presence of respiratory symptoms	1.300	0.357	13.289	3.671 (1.824–7.387)	<0.001
Distribution of middle/lower lobe	1.419	0.321	19.600	4.134 (2.206–7.750)	<0.001
Irregular shape	1.083	0.385	7.922	2.953 (1.389–6.277)	0.005
Density of PSNs	1.163	0.320	13.201	3.199 (1.708–5.991)	<0.001
CT value of GGO areas <−657 Hu	1.915	0.328	34.003	6.787 (3.566–12.919)	<0.001
Presence of abnormal intra-nodular vessel sign	1.589	0.374	17.996	4.897 (2.350–10.201)	<0.001
Presence of interlobular septal thickening	2.583	0.834	9.588	13.238 (2.581–67.906)	0.002
Constant	−4.631	0.400	134.273	0.010 (Na)	<0.001

Abbreviations: SSNs, subsolid nodules; PSNs, part-solid nodules; CT, computed tomography; GGO, ground-glass opacity; Na, not available.

with nonabsorbable inflammatory SSNs (all $P < 0.05$). The logistic regression function ($P=1/(1+e^{4.631-1.300*\text{respiratory symptoms}-1.419*\text{distribution of middle/lower lobe}-1.083*\text{irregular shape}-1.163*\text{density of PSNs}-1.915*\text{CT value of GGO areas <−657 Hu}-1.589*\text{abnormal intra-nodular vessel sign}-2.583*\text{interlobular septal thickening}})$) obtained an AUC (95% CI), accuracy, sensitivity, and specificity of 0.843 (95% CI: 0.811–0.872), 89.76%, 72.86%, and 81.23%, respectively. The internal validation cohort obtained an AUC (95% CI), accuracy, sensitivity, and specificity of 0.830 (95% CI: 0.759–0.887), 83.56%, 73.91%, and 76.42%, respectively.

CT–Pathological Correlations

After surgery, CT images of inflammatory and malignant SSNs were correlated with pathological findings. For inflammatory SSNs, GGO was found to correspond to slight interstitial fibrous tissue hyperplasia with inflammatory cell infiltration with or without exudation filling in the alveolar space, while solid density correlated to granuloma formation, organization in alveolar space, or obvious interstitial fiber hyperplasia with inflammatory cell infiltration (Figure 2). For malignant SSNs, GGO was found to be related to the invasion of tumor cells along pre-existing alveolar structures but not completely filling the alveolar space, while the solid component was associated with minimal invasion of tumor cells, alveolar collapse, and fibrosis (Figure 3).

Abnormal intra-nodular vessel sign in inflammatory SSNs corresponded to thickening of vessel walls with slight proliferation of fibrous tissue and exudation of alveolar space surrounding vessels (Figure 4), while that in malignant SSNs corresponded to the proliferation of fibrous tissue surrounding vessels with or without invasion of tumor cells (Figure 5).

Discussion

For patients with SSNs, an accurate preoperative diagnosis can help clinicians select the optimal therapeutic strategy and avoid unnecessary surgical resection of nonabsorbable inflammatory SSNs. In this study, we first compared the clinical and CT features of 70 patients with nonabsorbable inflammatory SSNs and 506 patients with malignant SSNs. We then developed and validated a multivariable logistic regression model for differentiating nonabsorbable inflammatory and

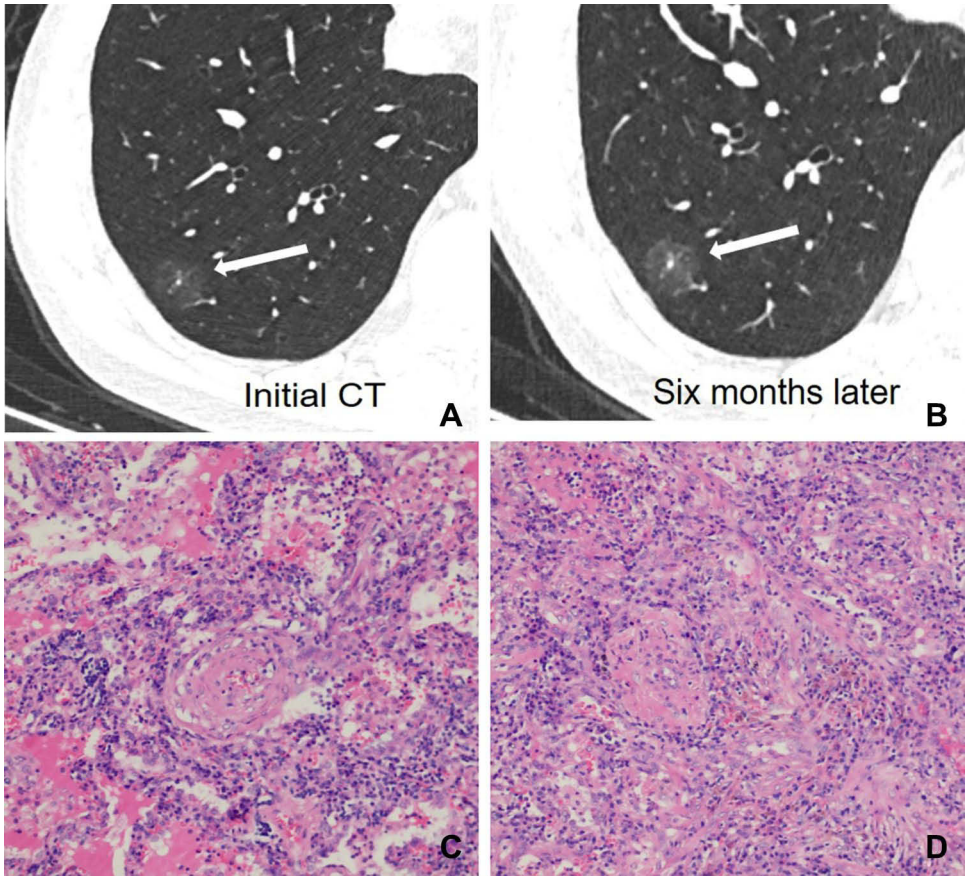

Figure 2 A 52-year-old man with a nonabsorbable inflammatory nodule. (**A**) CT image shows a part-solid ground glass opacity nodule with regular shape, ill-defined margin, and target sign in the right lower lobe (white long arrow); (**B**) CT images show a persistent nodule after six months follow-up CT (white long arrow); (**C**) photomicrograph shows that GGO corresponds to slightly interstitial fibrous tissue hyperplasia with inflammatory cell infiltration and with serous exudation in the alveolar space (hematoxylin-eosin stain, original magnification, ×100); (**D**) photomicrograph shows that the solid component corresponds to interstitial fiber hyperplasia with inflammatory cell infiltration (hematoxylin-eosin stain, original magnification, ×100).

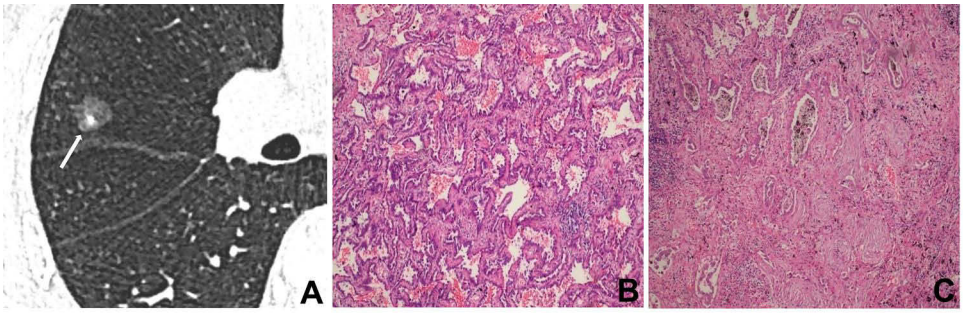

Figure 3 A 55-year-old man with minimally invasive adenocarcinoma. (**A**) CT image shows a part-solid nodule with regular shape and well-defined margin in the right middle lobe (white long arrow); (**B**) photomicrograph shows that GGO corresponds to tumor cells growing along the alveolar wall but not completely filling the alveolar space (hematoxylin-eosin stain; original magnification, ×100); (**C**) photomicrograph shows that a solid component corresponds to invasion of tumor cells and fibrosis (hematoxylin-eosin stain; original magnification, ×100).

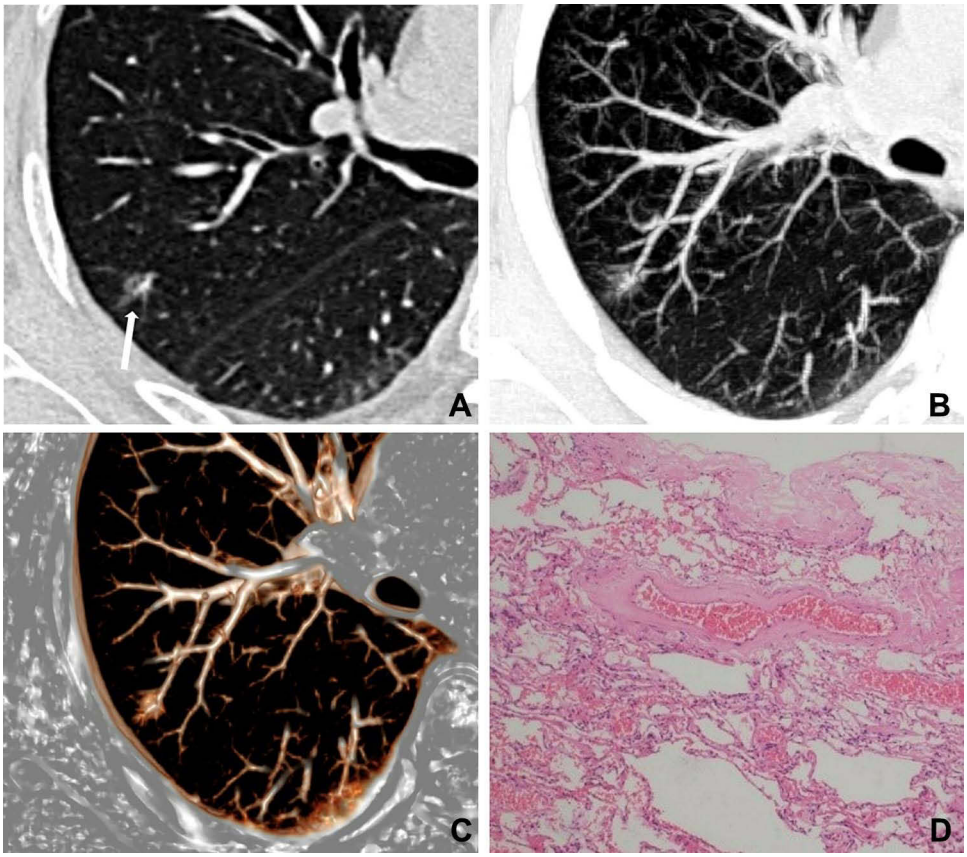

Figure 4 A 71-year-old woman with a nonabsorbable inflammatory nodule. (**A**) CT image shows a pure ground-glass nodule in the right upper lobe (white long arrow); (**B** and **C**) maximum intensity projection and volume rendering images show dilatation of intra-nodular vessels; (**D**) photomicrograph shows that the dilated vessels corresponded to the thickening of vessel walls with slight proliferation of fibrous tissue surrounding vessels (hematoxylin-eosin stain, original magnification, ×100).

malignant SSNs, and further explored the pathological basis of several important imaging features. This retrospective analysis produced several major findings.

For clinical characteristics, this study showed that no significant difference was observed in patient's age between the two groups. Previous research has shown that patients with lung cancer tend to be older than those with inflammatory lesions, possibly because increasing age comes with increasing incidence of malignancy due to decreased immune function and added total exposure to carcinogens;[16,17] however, those results are not consistent with our findings. The conflicting results among studies may be related to differences in sample size and study design. Furthermore, we found

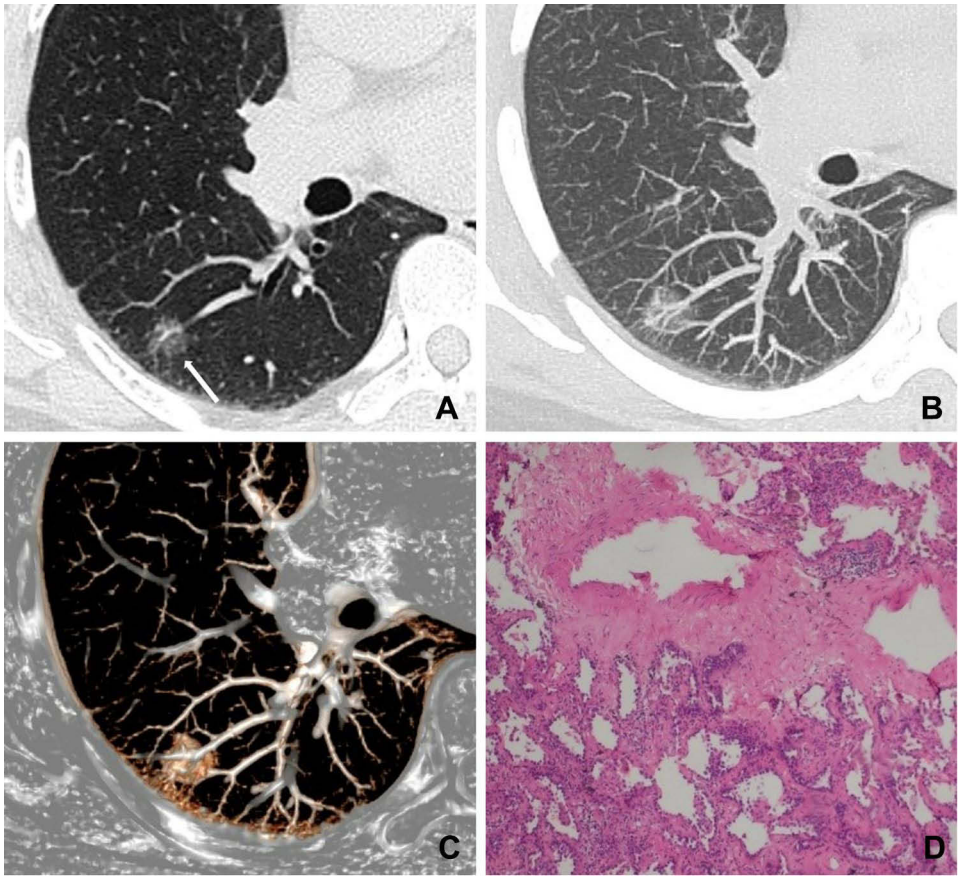

Figure 5 A 48-year-old woman with minimally invasive adenocarcinoma. (**A**) CT image shows a pure ground-glass nodule in the right lower lobe (white long arrow); (**B** and **C**) maximum intensity projection and volume rendering images show dilatation of intra-nodular vessels; (**D**) photomicrograph shows that the dilated vessels correspond to the proliferation of fibrous tissue surrounding vessels with invasion of tumor cells (hematoxylin-eosin stain, original magnification, ×100).

that patients with malignant SSNs were predominantly women and non-smokers. Arenberg[18] indicated that indolent lung adenocarcinoma that predominantly manifested as SSN was more common in non-smoking women, similar to our results. Moreover, this study found that more patients with nonabsorbable inflammatory SSNs had respiratory symptoms, mainly including cough, sputum, and chest pain. Choi et al[19] reported that the presence of respiratory symptoms was associated with benign diseases, mainly including inflammatory lesions and tuberculosis, which corroborated our results.

For CT features, we found that malignant SSNs were predominantly located in the upper lobe, which was consistent with the findings of some previous studies.[16,20] Our results indicated that, compared with inflammatory nodules, more malignant nodules had a regular shape, well-defined margin, and pGGN performance with a greater CT value of GGO areas. These findings could likely be attributed to differences in the pathological basis between inflammatory and malignant SSNs. Pathologically, GGO in inflammatory SSNs was associated with exudation filling in the alveolar space, which tended to result in an irregular shape, vague edge, and a low density of GGO areas on CT.[17,21] Contrastingly, GGO in malignant SSNs was related to minimal invasion of tumor cells along pre-existing alveolar structures but not completely filling the alveolar space, which might easily cause a regular shape, clear edge, and a relatively high density of GGO areas on CT. Previous research found that a regular shape and a well-defined-but-coarse interface were more common in malignant nodules than those in inflammatory ones,[22,23] with our results showing the same. Additionally, Yu et al[24] found that the possibility of malignancy is significantly increased with a high CT value, and that surgical treatment should thus be considered in those cases.

The current study revealed an interesting CT sign, namely, the target sign, which has not been described previously. This pattern was commonly detected in inflammatory nodules and manifested as a focal and round-like solid component in the center of GGO-predominant nodules, similar to a target. This finding may be a consequence of granuloma

formation in the central area, slight interstitial fibrous tissue hyperplasia with inflammatory cell infiltration with or without exudation of alveoli in the peripheral area. Unlike inflammatory PSNs, we found that the solid component in malignant PSNs predominantly appeared as an irregular shape with a scattered or eccentric distribution, which was consistent with previous results.[25–28] We also found that the intra-nodular vessel sign which could be evaluated only in SSNs was frequently observed in both groups, which was in agreement with the findings of Gao et al[3] and Fu et al[29] who showed that intra-nodular vessels can be observed in both inflammatory and malignant nodules. Furthermore, Gao et al[3,30] indicated that abnormal changes of the blood vessels passing through the nodules are highly suggestive of malignancy. However, we found that abnormal intra-nodular vessel sign was more common in inflammatory SSNs, which differs from the findings of some scholars. The reason for this result may be that previous studies primarily focused on invasive adenocarcinoma, for which more blood supply is needed to maintain the rapid growth of tumor cells. Thus, tumor cells will produce abundant vascular endothelial growth factor to promote angiogenesis, leading to an increase in neovascularization within tumors and concomitant vascular abnormalities.[31,32] In the present study, all patients had AIS and MIA, which were considered to have a slow growth rate, and angiogenesis in this stage was less obvious compared with that of invasive adenocarcinoma; thus, the incidence of abnormal intra-nodular vessel sign was accordingly lower. For inflammatory nodules, inflammatory mediators may cause abnormal changes, such as vasodilation and hyperpermeability, resulting in a higher percentage of abnormal intra-nodular vessel sign.[33–35] Therefore, the frequencies of abnormal intra-nodular vessel sign are distinctive among tumors with different invasiveness, suggesting that this sign should be analyzed separately according to the proportion of solid components on CT, which is closely related to tumor invasiveness.

Our study indicated that interlobular septal thickening is a frequent manifestation around inflammatory SSNs. Chung et al[36] reported that common diseases, such as pulmonary edema, pneumonias, and pulmonary fibrosis, cause interlobular septal thickening. For inflammatory nodules, this sign may be attributed to inflammation affecting the septa.

Multiparametric analysis indicated that presence of respiratory symptoms, distribution of middle/lower lobe, PSNs, irregular shape, CT value of GGO areas < −657 Hu, presence of abnormal intra-nodular vessel sign, and interlobular septal thickening were the most effective factors for diagnosing nonabsorbable inflammatory SSNs. This model obtained an AUC and accuracy of 0.843 and 89.76%, respectively. The internal validation cohort also indicated a good performance. Familiarity with these differential features may improve diagnostic accuracy of SSNs with a solid component ≤5 mm.

There were several limitations to this study. First, given that most inflammatory nodules are absorbable and all the patients included in the current study underwent surgical resection, there may be some selection bias. Second, the number of patients with nonabsorbable inflammatory SSNs was small. Third, the CT features of nodules are easily affected by CT acquisition and reconstruction so that the results need to be verified in future studies. Forth, exact matching of the histopathological slice to the imaging slice was very difficult, and further correlation studies with a larger sample size are warranted.

Conclusion

In conclusion, our findings demonstrate that nonabsorbable inflammatory and malignant SSNs have different clinical and radiological characteristics. Specifically, SSNs with respiratory symptom, a middle/lower distribution, irregular shape, PSNs density, CT value of GGO areas <−657 Hu, abnormal intra-nodular vascular, and interlobular septal thickening are high suggestive of nonabsorbable inflammatory nodule and follow-up CT should be considered first. A good understanding of these features and pathological basis can contribute to the accurate diagnosis of SSNs, reduction in the number of unnecessary surgeries, and advancements in determining an optimal treatment strategy.

Abbreviations

SSNs, subsolid nodules; CT, computed tomography; pGGNs, pure ground-glass opacity nodules; PSNs, part-solid nodules; GGO, ground-glass opacity; AIS, adenocarcinoma in situ; MIA, minimally invasive adenocarcinoma; ROC, receiver operating characteristic; AUC, area under the curve; OR, odds ratio; CI, confidence interval.

Data Sharing Statement

Data supporting the results reported in the manuscript can be found by contacting the correspondence author with email (liqi89011721@163.com).

Ethics Approval and Informed Consent

The First Affiliated Hospital of ChongQing Medical University's institutional review board approved this study (approval number: 2019-062), and the need for informed consent was waived due to its retrospective nature.

Consent for Publication

The details of any images, recordings, and figures can be published, and the persons providing consent have been shown the article contents to be published.

Author Contributions

All authors made a significant contribution to the work reported, whether that is in the conception, study design, execution, acquisition of data, analysis and interpretation, or in all these areas; took part in drafting, revising or critically reviewing the article; gave final approval of the version to be published; have agreed on the journal to which the article has been submitted; and agree to be accountable for all aspects of the work.

Funding

This study has received funding by Chongqing Science and Technology Commission (cstc2017jcyjAX0281 and cstc2016shms-ztzx10002) and Chongqing Health and Family Planning Commission (2022MSXM147) of China, and the sponsors had no involvement in the role of this manuscript.

Disclosure

The authors report no conflicts of interest in this work.

References

1. Kobayashi Y, Ambrogio C, Mitsudomi T. Ground-glass nodules of the lung in never-smokers and smokers: clinical and genetic insights. *Transl Lung Cancer Res*. 2018;7(4):487–497. doi:10.21037/tlcr.2018.07.04
2. Naidich DP, Bankier AA, MacMahon H, et al. Recommendations for the management of subsolid pulmonary nodules detected at CT: a statement from the Fleischner Society. *Radiology*. 2013;266(1):304–317. doi:10.1148/radiol.12120628
3. Gao F, Li M, Ge X, et al. Multi-detector spiral CT study of the relationships between pulmonary ground-glass nodules and blood vessels. *Eur Radiol*. 2013;23(12):3271–3277. doi:10.1007/s00330-013-2954-3
4. Shima T, Kinoshita T, Sasaki N, et al. Feasibility of intraoperative diagnosis of lung adenocarcinoma in situ to avoid excessive resection. *J Thorac Dis*. 2021;13(3):1338–1346. doi:10.21037/jtd-20-2710
5. Godoy MC, Naidich DP. Subsolid pulmonary nodules and the spectrum of peripheral adenocarcinomas of the lung: recommended interim guidelines for assessment and management. *Radiology*. 2009;253(3):606–622. doi:10.1148/radiol.2533090179
6. Sato Y, Fujimoto D, Morimoto T, et al. Natural history and clinical characteristics of multiple pulmonary nodules with ground glass opacity. *Respirology*. 2017;22(8):1615–1621. doi:10.1111/resp.13089
7. Ye T, Deng L, Xiang J, et al. Predictors of pathologic tumor invasion and prognosis for ground glass opacity featured lung adenocarcinoma. *Ann Thorac Surg*. 2018;106(6):1682–1690. doi:10.1016/j.athoracsur.2018.06.058
8. Eguchi T, Kadota K, Park BJ, et al. The new IASLC-ATS-ERS lung adenocarcinoma classification: what the surgeon should know. *Semin Thorac Cardiovasc Surg*. 2014;26(3):210–222. doi:10.1053/j.semtcvs.2014.09.002
9. Yan T, Wang K, Liu J, et al. Wedge resection is equal to segmental resection for pulmonary typical carcinoid patients at localized stage: a population-based analysis. *Peer J*. 2019;7:e7519. doi:10.7717/peerj.7519
10. Torpy JM, Lynm C, Glass RM. JAMA patient page Lung complications after surgery. *JAMA*. 2009;302(14):1610. doi:10.1001/jama.302.14.1610
11. Travis WD, Brambilla E, Noguchi M, et al. International association for the study of lung cancer/American thoracic society/European respiratory society international multidisciplinary classification of lung adenocarcinoma. *J Thorac Oncol*. 2011;6(2):244–285. doi:10.1097/JTO.0b013e318206a221
12. Lee KH, Goo JM, Park SJ, et al. Correlation between the size of the solid component on thin-section CT and the invasive component on pathology in small lung adenocarcinomas manifesting as ground-glass nodules. *J Thorac Oncol*. 2014;9(1):74–82. doi:10.1097/JTO.0000000000000019
13. Revel MP, Mannes I, Benzakoun J, et al. Subsolid lung nodule classification: a CT criterion for improving interobserver agreement. *Radiology*. 2018;286(1):316–325. doi:10.1148/radiol.2017170044

14. Detterbeck FC, Chansky K, Groome P, et al. The IASLC lung cancer staging project: methodology and validation used in the development of proposals for revision of the stage classification of NSCLC in the forthcoming (eighth) edition of the TNM classification of lung cancer. *J Thorac Oncol*. 2016;11(9):1433–1446. doi:10.1016/j.jtho.2016.06.028
15. Detterbeck FC, Boffa DJ, Kim AW, et al. The eighth edition lung cancer stage classification. *Chest*. 2017;151(1):193–203. doi:10.1016/j.chest.2016.10.010
16. Chu ZG, Sheng B, Liu MQ, et al. Differential diagnosis of solitary pulmonary inflammatory lesions and peripheral lung cancers with contrast-enhanced computed tomography. *Clinics*. 2016;71(10):555–561. doi:10.6061/clinics/2016(10)01
17. Lin RY, Lv FJ, Fu BJ, et al. Features for predicting absorbable pulmonary solid nodules as depicted on thin-section computed tomography. *J Inflamm Res*. 2021;14:2933–2939. doi:10.2147/JIR.S318125
18. Arenberg D. Bronchioloalveolar lung cancer: ACCP evidence-based clinical practice guidelines (2nd edition). *Chest*. 2007;132(3 Suppl):306S–313S. doi:10.1378/chest.07-1383
19. Choi SM, Heo EY, Lee J, et al. Characteristics of benign solitary pulmonary nodules confirmed by diagnostic video-assisted thoracoscopic surgery. *Clin Respir J*. 2016;10(2):181–188. doi:10.1111/crj.12200
20. Xiao YD, Lv FJ, Li WJ, et al. Solitary pulmonary inflammatory nodule: CT features and pathological findings. *J Inflamm Res*. 2021;14:2741–2751. doi:10.2147/JIR.S304431
21. Kim HY, Shim YM, Lee KS, et al. Persistent pulmonary nodular ground-glass opacity at thin-section CT: histopathologic comparisons. *Radiology*. 2007;245(1):267–275. doi:10.1148/radiol.2451061682
22. Chu ZG, Li WJ, Fu BJ, et al. CT characteristics for predicting invasiveness in pulmonary pure ground-glass nodules. *AJR Am J Roentgenol*. 2020;215(2):351–358. doi:10.2214/AJR.19.22381
23. Fan L, Liu SY, Li QC, et al. Multidetector CT features of pulmonary focal ground-glass opacity: differences between benign and malignant. *Br J Radiol*. 2012;85(1015):897–904. doi:10.1259/bjr/33150223
24. Yu J, Zhu S, Ge Z, et al. Multislice spiral computed tomography in the differential diagnosis of ground-glass opacity. *J Cancer Res Ther*. 2018;14(1):128–132. doi:10.4103/jcrt.JCRT-660-17
25. Li WJ, Lv FJ, Tan YW, et al. Pulmonary benign ground-glass nodules: CT features and pathological findings. *Int J Gen Med*. 2021;14:581–590. doi:10.2147/IJGM.S298517
26. Travis WD, Garg K, Franklin WA, et al. Evolving concepts in the pathology and computed tomography imaging of lung adenocarcinoma and bronchioloalveolar carcinoma. *J Clin Oncol*. 2005;23(14):3279–3287. doi:10.1200/JCO.2005.15.776
27. Yoshida Y, Yanagawa M, Hata A, et al. Quantitative volumetry of ground-glass nodules on high-spatial-resolution CT with 0.25-mm section thickness and 1024 matrix: phantom and clinical studies. *Eur J Radiol Open*. 2021;8:100362. doi:10.1016/j.ejro.2021.100362
28. Lee SM, Park CM, Song YS, et al. CT assessment-based direct surgical resection of part-solid nodules with solid component larger than 5 mm without preoperative biopsy: experience at a single tertiary hospital. *Eur Radiol*. 2017;27(12):5119–5126. doi:10.1007/s00330-017-4917-6
29. Fu BJ, Lv FJ, Li WJ, et al. Significance of intra-nodular vessel sign in differentiating benign and malignant pulmonary ground-glass nodules. *Insights Imaging*. 2021;12(1):65. doi:10.1186/s13244-021-01012-7
30. Gao F, Sun Y, Zhang G, et al. CT characterization of different pathological types of subcentimeter pulmonary ground-glass nodular lesions. *Br J Radiol*. 2019;92(1094):20180204. doi:10.1259/bjr.20180204
31. Ayten O, Tas D, Demirer E, et al. Angiopoietin 2 levels in serum and bronchial lavage fluids and their relationship with cancer stages in lung cancer patients. *Thorac Cancer*. 2013;4(1):20–26. doi:10.1111/j.1759-7714.2012.00128.x
32. Xuan ZX, Zhang S, Yuan SJ, et al. Prognostic value of angiopoietin-2 in non-small cell lung cancer patients: a meta-analysis. *World J Surg Oncol*. 2016;14(1):237. doi:10.1186/s12957-016-0992-4
33. Chen L, Deng H, Cui H, et al. Inflammatory responses and inflammation-associated diseases in organs. *Oncotarget*. 2018;9(6):7204–7218. doi:10.18632/oncotarget.23208
34. Li Q, Huang XT, Li CH, et al. CT features of coronavirus disease 2019 (COVID-19) with an emphasis on the vascular enlargement pattern. *Eur J Radiol*. 2021;134:109442. doi:10.1016/j.ejrad.2020.109442
35. Liu J, Zheng X, Tong Q, et al. Overlapping and discrete aspects of the pathology and pathogenesis of the emerging human pathogenic coronaviruses SARS-CoV, MERS-CoV, and 2019-nCoV. *J Med Virol*. 2020;92(5):491–494. doi:10.1002/jmv.25709
36. Chung MJ, Lee KS, Franquet T, et al. Metabolic lung disease: imaging and histopathologic findings. *Eur J Radiol*. 2005;54(2):233–245. doi:10.1016/j.ejrad.2004.07.003